Tribology Letters (2019) 67:40
https://doi.org/10.1007/s11249-019-1153-z

ORIGINAL PAPER

Effect of Retained Austenite on White Etching Crack Behavior of Carburized AISI 8620 Steel Under Boundary Lubrication

Sougata Roy[1] · Benjamin Gould[2] · Ye Zhou[2,3] · Nicholaos G. Demas[2] · Aaron C. Greco[2] · Sriram Sundararajan[1]

Received: 26 October 2018 / Accepted: 26 February 2019

Abstract
The formation of white etching cracks (WECs) is a dominant failure mode in wind turbine gearbox bearings that can significantly shorten their operating life. Although the phenomenon of WECs has been communicated in the field for more than a decade, the driving mechanisms are still debated, and the impact of proposed mitigation techniques is not quantified. Leading hypotheses to inhibit the formation of WECs center on material solutions, including the use of steel with high levels of retained austenite (RA). The present work aims to explore the impact of RA on the formation of WECs within AISI 8620 steel under boundary lubrication. A three ring-on-roller benchtop test rig was used to replicate WECs in samples with different levels of RA. While varying levels of RA had a minimal effect on time until failure, a significant effect on crack morphology was observed. Additionally, potential underlying mechanisms of White Etching Area formation were elucidated. Under the current test conditions, the microstructural alterations adjacent to the cracks in the lower RA samples were more developed compared to those of the higher RA samples. Additionally, the WEC networks in the high RA samples contained significantly more crack branches than those of the low RA samples.

Keywords White etching cracks · Retained austenite · Rolling contact fatigue · Wind turbine gearbox bearings · Microstructural alterations · Bearing failure

1 Introduction

Industrial scale drivetrain bearings, particularly those used in wind turbines, often exhibit premature macropitting or spalling well before reaching their rolling contact fatigue (RCF) design life [1–4]. In many of these cases, the premature failures are caused by broad-branching crack networks surrounded by local regions of nano-grained, microstructurally altered steel [5–9]. When bearings failed as the aforementioned cracks are metalographically prepared and etched with Nital (nitric acid and ethanol), the nano-grained regions resist the etchant, and appear white in contrast with the surrounding matrix steel. Because of this appearance, these failures are often referred to as "White etching cracks" (WECs). Figure 1 shows a damaged bearing, and a section of the WEC network which caused the damage.

A general common root cause of WEC networks in field bearings is still unknown. However, the microstructural alterations that appear in conjunction with the cracks must form due to local excess in energy causing recrystallization or atomic diffusion. Previous researchers have attributed the formation of WECs to multiple drivers, including applied strain due to normal loading [11–25], torque reversals leading to impacts [19, 20, 26], tensile frictional stresses at the contact surface [27], electrical discharge [28], sliding contacts induced via acceleration or under-loading [29–31], and hydrogen release from degraded or contaminated lubricants [17, 32, 33]. Because no consensus exists on WEC drivers in the field, researchers have taken multiple avenues with regard to recreating these crack networks in benchtop tests. These efforts include pre-charging test samples with hydrogen [23, 34–49], the use of specific lubricant formulations thought to promote the formation of WECs [10, 25, 50–57], grain boundary embrittlement induced via heat treatment [58], excessive slip [10, 25, 59, 60], the application

✉ Sriram Sundararajan
srirams@iastate.edu

[1] Department of Mechanical Engineering, Iowa State University, Ames, IA 50011, USA

[2] Applied Materials Division, Argonne National Laboratory, Argonne, IL 60439, USA

[3] State Key Laboratory of Mechanical Transmissions, Chongqing University, Chongqing 400030, China

Published online: 03 March 2019

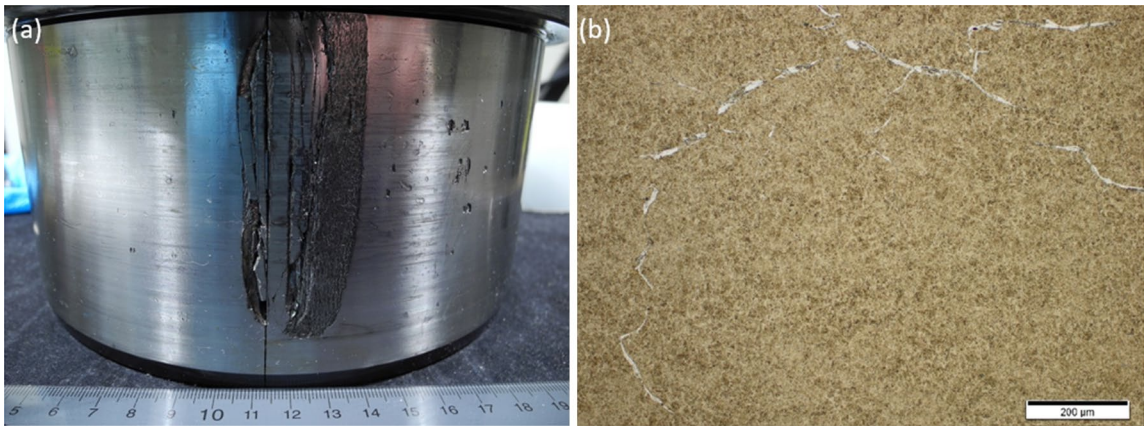

Fig. 1 **a** A failed high-speed shaft bearing pulled from a wind turbine, and **b** a section of the WEC network which caused the failure. Image taken from [10]

of external electrical load [28], and impact loading [61]. In-depth reviews of the leading hypotheses as to the factors responsible for the formation of WECs can be found in [18, 62]. While there are many unknowns surrounding WECs, recent analysis by Gould et al. [62, 63] elucidated many of the formation mechanisms of these crack networks within field bearings. Gould et al. used X-ray tomography to investigate the morphology of newly initiated WECs. It was found that the WECs studied initiated in the subsurface of bearings, preferentially at inclusions that contained both aluminum oxide and manganese sulfide components. Additionally, it was found that formation of a crack is a prerequisite to the formation of microstructural alterations [63]. The findings are further supported by the observation of WEC interactions with non-metallic inclusions of oxide and MnS at serial-sectioned wind turbine field bearings [23], and also benchtop testing with metallographic serial sectioning of entire WECs also showed the same interactions with the WECs often being contained entirely within the subsurface without any contact surface connections [55]. This suggests that efforts to mitigate the formation of WECs should focus on combating the formation of subsurface crack networks.

Industry has proposed multiple solutions that aim to eliminate the formation of WECs. These include the use of soft black oxide conversion layers to protect bearings from embrittlement stemming from contamination or lubricant decomposition, the use of hard coatings, such as diamond-like carbon, to mitigate the formation of nascent steel surfaces, the use of case carburization to impede subsurface crack initiation and propagation, and the use of specific steel microstructures, particularly those rich in retained austenite (RA), to inhibit cracking [64–66]. Evans detailed several methods which have been proposed by different researchers to mitigate WECs at industrial fields and remaining challenges [18]. While numerous proposed solutions exist, the public literature is severely lacking when it comes to quantifying the effectiveness of each of these solutions. Recent studies by Roy and Sundararajan have investigated the effect of RA content on specific tribological failure modes including micropitting [67] and spalling [68]. The aim of the current work is to conduct a follow-on study using the spalled samples from [68], in order to quantify the effect of RA on the formation of WECs, both in terms of failure rate, and crack morphology.

2 Material

2.1 Sample Preparation and Characterization

The fundamental techniques used to prepare samples with a wide range of RA were by (a) varying carbon potential during carburizing and (b) varying tempering time and temperature during tempering step. Decreased martensite start and finish temperature due to increasing carbon potential results in an incomplete conversion of austenite to martensite, which leads to higher RA content in the final microstructure [69]. Increasing tempering temperature and time can lead to conversion of existing RA to other phases such as bainite or pearlite [70]. A Cu-Kα X-ray diffractometer (Model: Rigaku SmartLab with micro-diffraction and sample mapping attachment) was used to measure the baseline RA content of the prepared samples. Residual stress levels were measured using a Cr-X-ray diffractometer. A 35-kV accelerating voltage and 1.5 mA current were used to measure residual stress of near surface region (depth approximately 0.025 mm). A position-sensitive proportional counter detector was used to efficiently collect XRD spectra at different tilt angles. Please refer to our previous publication [68] for the detailed discussion on sample preparation and baseline material characterization. Average levels of RA% in three batches of samples

were approximately 0%, 15%, and 70% with compressive residual stress levels of 493.3 ± 11.3, 251 ± 42.9, and 153.2 ± 49.3 MPa. In this paper, 0%, 15%, and 70% RA levels are mentioned as low, medium, and high RA samples. A higher residual stress level was observed in lower RA samples due to two reasons. First, higher temperature tempering helped to convert remaining austenite after quenching to other phases which induced compressive residual stress due to volumetric expansion. Second, tempering at higher temperature also could result in thermal-induced residual stress. As a result, lower RA samples showed higher baseline residual stress. The samples were eventually ground and polished to achieve a similar range of surface roughness (R_a 0.22 ± 0.02 µm for scan size 1 mm × 0.6 mm).

2.2 Microhardness Tests

The resulting subsurface hardness for each heat treatment was determined by probing an untested roller at multiple points below the contact surface using a Vickers micro-indenter with a mass of 400 g at an average spacing of around 100 µm. These data are shown in Fig. 2. It can be observed that the near surface hardness of the low RA sample was less than the medium and high RA sample due to the higher tempering temperature used during sample preparation. Additionally, the hardness of the high RA sample actually increased with depth below the contact surface, until a depth of around 400 µm. The authors hypothesize that the reason for this increase is that the amount of diffused carbon decreased with depth below the contact surface due to the carburizing heat treatment. Therefore, within the case layer, the amount of hard martensite increased with depth, and the amount of softer RA decreased with depth.

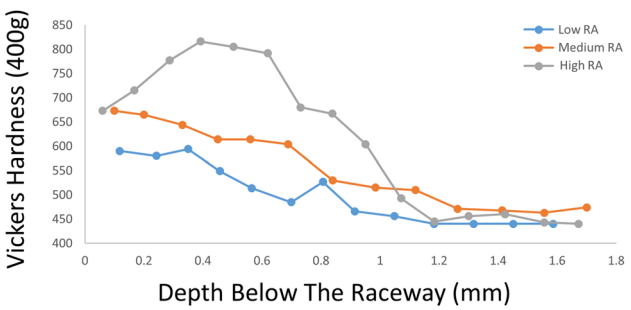

Fig. 2 A chart showing the measured hardness of rollers of varying heat treatment vs depth below the raceway surface. The hardness was measured at multiple points using a Vickers micro-indenter with a load of 400 g

3 Experimental Methods

3.1 Benchtop RCF Experiments

A benchtop test rig (micropitting rig manufactured by PCS Instruments) was used to conduct RCF experiments on different RA samples [67]. The same test rig can be used to replicate different failure modes of RCF such as micropitting [67, 71], spalling [68], and WEC formation [10, 25] under different lubrication and operating conditions. Spalling is the formation of a macropit on the surface of a sample due to many forms of crack initiation (e.g., classical subsurface RCF, surface initiated RCF, or WECs). However, a WEC does not need to lead to a spall to be considered a WEC. Many tests can run from millions of cycles with a WEC in the subsurface before the formation of a spall. A brief summary of the test rig and testing conditions to replicate spalling conditions use to generate the samples analyzed in this study is provided below. Additional details of these aspects are described in [68]. The test rig is shown in Fig. 3a and can simulate rolling–sliding contact under different test conditions by varying the entrainment velocity, test specimen speed, lubricating oil temperature, and operating load. Figure 3b, c shows the enlarged view of the test chamber and test sample (roller), respectively. The diameters of roller and rings were 12 mm and 54 mm, respectively, and for the present investigation, the material for both rings and rollers was carburized AISI 8620 steel. The objective of this study

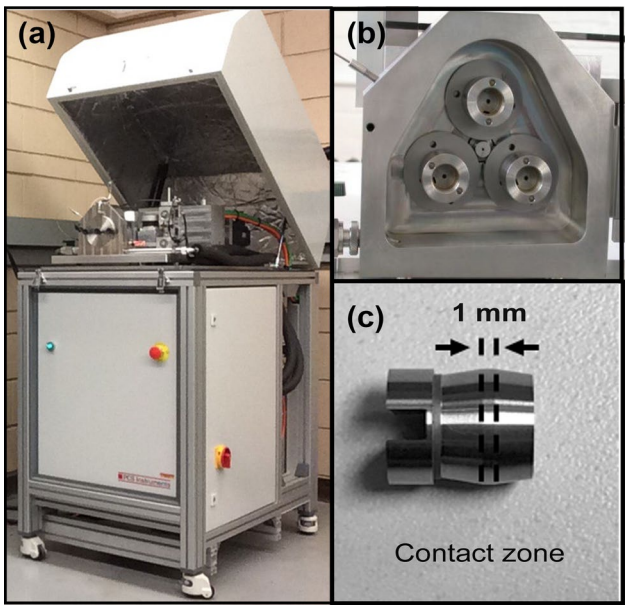

Fig. 3 **a** Experimental setup of micropitting test rig, **b** enlarged view of test chamber showing the rings and roller, and **c** image of a test specimen (roller)

was to analyze the WEC morphology of the samples failed at different RCF cycles due to WEC-induced spalling. The specific experimental conditions to replicate WECs on different RA samples were the same and are as follows: entrainment velocity 1 m/s, slide-to-roll ratio (SRR) − 30% (ring velocity was lower than roller velocity), maximum Hertzian contact pressure 1.9 GPa, lubricant sump temperature 80 °C with a minimum oil-film thickness of 51 nm (based on Pan–Hamrock's equation for line contact [68]). These test conditions were chosen because they were previously shown to accelerate the formation of WECs in the MPR [10, 25].

The operating conditions of gearboxes in wind turbines are extremely stochastic due to the ever-changing input wind load. This results in significant differences in bearing rotational speed as well as instances of high sliding which can result in boundary lubrication ($\lambda < 1$). If the exact turbine conditions were used in the present test, then we would expect the failure of benchtop test specimens to occur over the same timeframe of bearings in the field (~ 5 years per test). As with any accelerated benchtop failure, exacerbated conditions are necessary to form the relevant failure in a timely manner. Thus, the lubrication regime for present test condition was boundary lubrication ($\lambda < 1$). An API group II base oil mixed with ZDDP and other additive packages was used as lubricant for the set of experiments. The oil was sheared prior to the experiments to avoid viscosity alteration due to shearing during the tests. The kinematic viscosity of the oil at 40° and 100 °C were 50.51–51.44 cSt and 7.56–7.81 cSt, respectively. The vibration signal was captured using an accelerometer. The test was stopped by reaching a peak to peak accelerometer signal of 10 g due to spall or macropit formation on sample surface.

3.2 White Etching Crack Characterization Protocol

At the end of every test, the respective rollers were sectioned in the circumferential-depth plane. Figure 4 shows a schematic describing the cross-sectional plan for observing WECs in different samples. Samples were then mounted in Bakelite, and polished to different depths along the contact zone using a series of polishing steps: 220 grit (grinding), 9 µm, 3 µm, and 1 µm diamond polishing solution. For every section, the samples were etched with a 3% Nital solution and the subsurface of each sample was examined for microstructural alterations using and optical microscope. When necessary, additional analysis was performed on an FEI Quanta 400F scanning electron microscope (SEM).

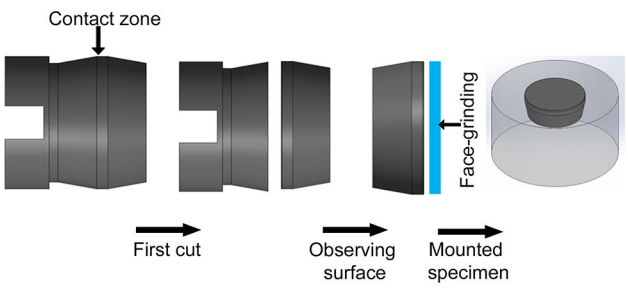

Fig. 4 Cross-sectional plan for WECs observation

4 Results

The results of the 10 fatigue tests which were previously conducted to study the spalling behavior of different RA samples are shown in [68]. Six of the spalled samples discussed in [68] were selected to further study the existence of WECs and subsurface crack morphology. The RCF test life of those six specific samples from three different RA levels is shown in Table 1.

The low RA test samples ran for comparative less number of cycles compared to the medium and high RA samples before the spall formed on surface triggering peak to peak accelerometer signal to 10 g. While there was no statistically significant difference in RCF life among medium and high RA samples, the medium RA samples had a slightly larger average time until failure. In all cases, the tests were automatically shut down due to the formation of a macropit or spall. Based on height maps of spalls occurred on different samples, the spalls were 100–120 µm deep [68] and covered almost the whole facewidth (contact region) of the rollers as showed in Fig. 5.

It was observed that the level of RA had a drastic effect on the morphology of the crack networks, as well as the White Etching Area (WEA) that accompanied them. The WEC networks that formed in the samples with higher levels of RA contained a larger number of crack branches as shown in Fig. 6. In addition, Fig. 7 shows that the WEA adjacent to the crack faces was more defined for samples with lower RA compared to the samples with higher RA.

Table 1 Number of cycles on roller before spalling

Samples	Test trials	RCF life (million)
High RA	Test 1	20.4
	Test 2	18.9
Medium RA	Test 3	23
	Test 4	22.3
Low RA	Test 5	16.3
	Test 6	12.2

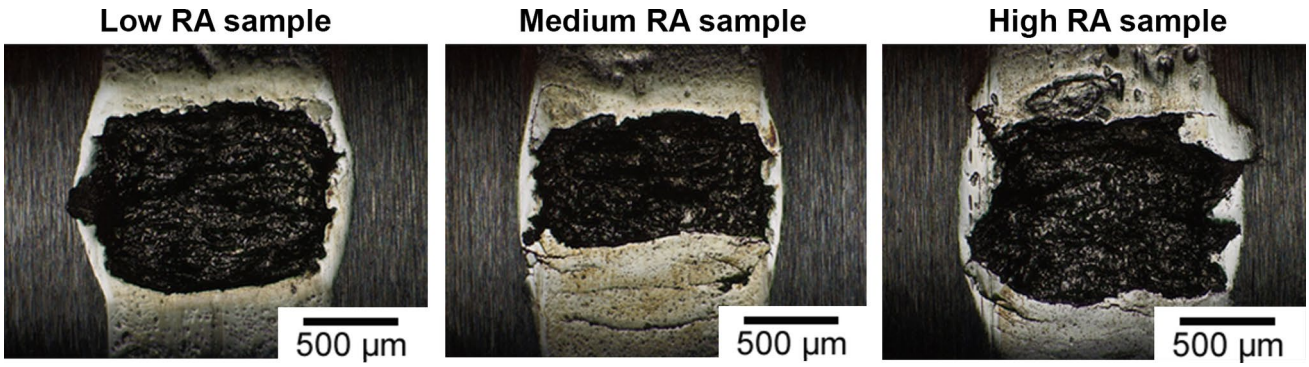

Fig. 5 Optical micrographs of formed spalls on failed test samples

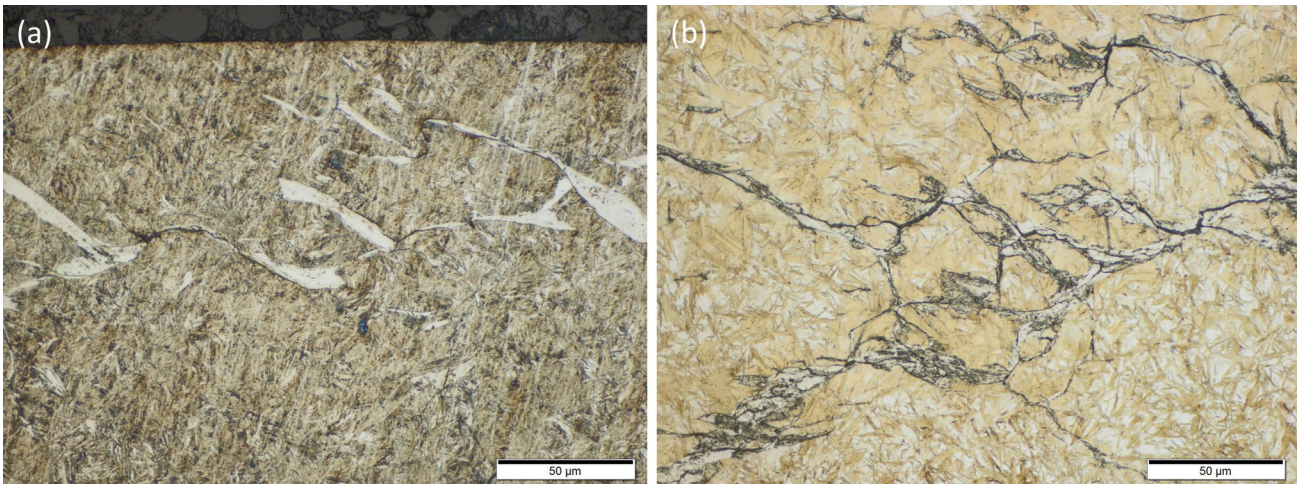

Fig. 6 **a** A WEC network observed within Test 6, a sample with a low level of RA and **b** a WEC network within Test 2, a sample with a high level of RA. These images show the increase in the branching nature of the WEC networks documented in the higher RA samples

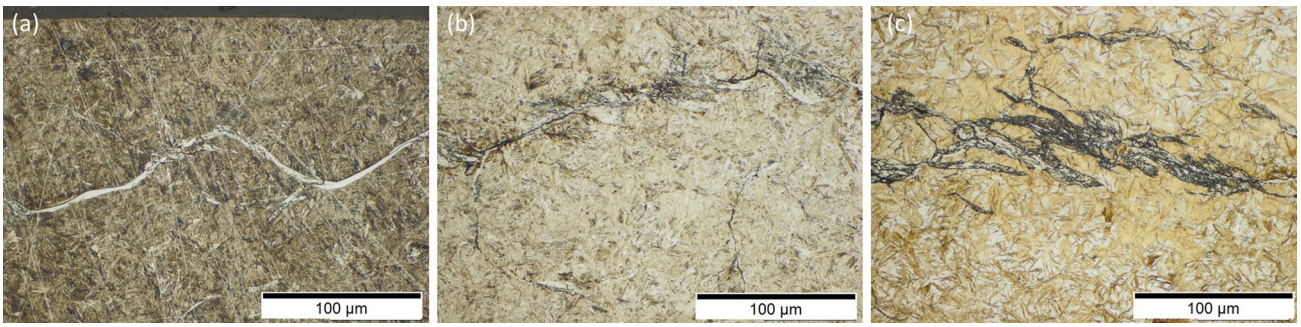

Fig. 7 Three images showing how increased levels of RA within samples led to changes in the appearance of the microstructural alterations which appear adjacent to the crack networks in each sample. **a** Test 5 (low RA), **b** Test 4 (mid RA), and **c** Test 2 (high RA). It was documented that the rollers which contained a lower level of RA formed WEA that was far more defined than that of the higher levels of RA

5 Discussion

5.1 Effect of RA on WEC Formation and Crack Morphology

As stated above, the method that was used to induce high levels of RA was supersaturating the outer layer of the samples with carbon. If enough carbon exists locally, and the steel is constrained from expanding in volume, then the microstructure of the steel must remain in the face-centered cubic (FCC) configuration of austenite as compared to the body-centered cubic (BCC) lattice of ferrite, or the body-centered tetragonal (BCT) lattice of martensite. This is due to the fact that the FCC configuration has a much higher carbon solubility limit than that of a BCC or BCT structure [72]. As crack networks propagate through the subsurface regions of the samples containing high amounts of RA, these networks interact with regions of RA. The spacing induced by the cracks allows for expiation of the region of RA and an instantaneous transformation of the FCC (austenite) to BCC or BCT (martensite). During this FCC to BCC or BCT phase transformation, volumetric expansion occurs, thereby generating a compressive stress in the surrounding regions. This increase in compressive residual stress due to contact induced damage was previously documented and correlated to the relative amount of material that underwent an austenitic to martensitic transformation [68]. As this transformation occurs locally, the new compressive stress induced by the transformation hinders the crack tip from further expansion in the same direction. As a result, the crack follows a new path of least resistance likely propagating in a different direction. The author hypothesizes that this is why larger amounts of crack branching were observed in the higher RA samples. Figure 8 supports this hypothesis. This figure shows two significantly branched crack networks within a high RA sample. As stated above, regions of RA appear white when etched. Within Fig. 8, it can be observed that steel adjacent to the crack network is devoid of RA, thereby indicating that the RA that has interacted with the crack network has undergone a transformation to martensite.

This hypothesis is further supported by surface residual stress levels taken before and after testing. The post-experiment compressive residual stress levels were 526.3 ± 29, 454.1 ± 17.1, and 513.5 ± 16.9 MPa for high, medium, and low RA samples, respectively. It can be observed that the residual stress levels had increased 3.4 and 1.8 times, respectively, for high and medium RA samples but the increase was insignificant for low RA samples. This increase in compressive residual stress is from synergistic impact of compressive stress build-up due to martensitic phase transformation at the rolling contact region and

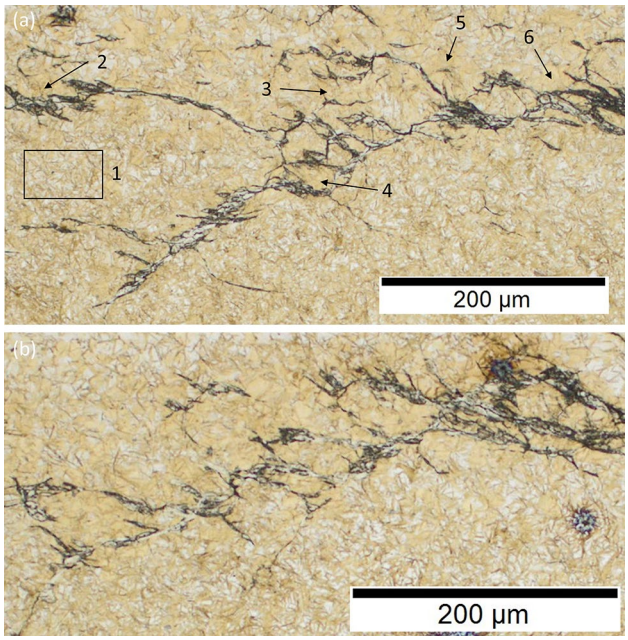

Fig. 8 **a** An image of a broad-branching WEC network within (Test 2). Zone *1* within this image shows the matrix microstructure, which is unaffected by the cracking failure. This zone shows large regions of lighter etching, corresponding to areas rich in RA. Regions *2–6*, which are all adjacent to crack faces, show a clear depletion of this lighter etching. This indicates that these regions have transformed from RA to martensite due to the presence of the crack. **b** Another WEC network within this sample, where it can be observed, similar to **a**, that the steel adjacent to the crack faces contains far less RA then the steel unaffected by the crack

near WEC tip regions which in turn results in significant crack branching. Also, at the end of the test, the highest RA sample had highest compressive residual stress. Thus, it can be hypothesized that difference in RA levels had more significant impact on crack branching compared to baseline residual stress level. Several researchers also previously pointed out about the build-up of compressive residual stress and fine martensite particles which resulted due to phase transformation of austenite near the crack tip region during RCF [73, 74] cycles.

It was also observed that the regions of WEA adjacent to the crack networks were less developed in the higher RA samples. This can be seen in Fig. 6 and in Fig. 7. The leading hypotheses as to why WEA forms adjacent to crack networks are based on the local accumulation of energy which leads to a gradual increase in the dislocation density [18, 25, 75, 76]. As the dislocation density increases, the dislocations rearrange to form new smaller cells, causing gradual grain refinement. The energy that drives this process likely comes from multiple origins, including strain-based energy release due to over-rolling, frictional energy generated due to sliding at the contact surface, and frictional energy generated at the crack interface due to crack face rubbing. The authors

have two theories as to why the samples with higher levels of RA contained less-developed WEAs than the samples with low levels of RA. The first theory is that the cracks contained within the higher RA samples had less time from initiation to a macropitting failure, and thus less time to accrue localized energy before a failure. This idea stems from the fact that the case layer of the medium and high RA samples was much harder, and therefore less tough, than the low RA samples. The second theory as to why these observable differences in WEA morphology occur has to do with differences in the rate of energy generated due to crack face rubbing. In the cases of WECs generated in steels with a low level of RA, such as the images shown in Figs. 6a, 7a as well as most 52100 through hardened steels, the WEAs adjacent to the crack networks are distinct and well defined. An SEM image showing a well-defined WEA within a low RA sample is shown in Fig. 9a. Within these well-defined WEAs, there are normally very few crack branches. Therefore, when the region is loaded, the imposed stress is concentrated on a single crack causing the two crack faces to be easily compressed together, the shear component of the stress state causes crack face rubbing, and subsequent energy is released which increases the dislocation density adjacent to the cracks. However, in the case of a crack network within a high RA sample, there are numerous crack branches within a local area for the reasons stated above. Therefore, when a region containing multiple crack networks is stressed, the numerous crack branches in a local area all compress to varying levels. In other words, there are significantly more degrees of freedom in terms of how the compression can be accommodated. Therefore, a multitude of cracks can take the various shear and compressive components of over-rolling, leading to a decrease in energy localization adjacent to any single crack face. Because of this, gradual microstructural alterations form adjacent to the numerous cracks in a local area, as opposed to well-defined microstructural alterations forming adjacent to one crack face. An example of a non-well-defined WEA within a high RA sample is shown in Fig. 9b.

6 Conclusions

Spalled or macropitted samples with a wide range RA were analyzed to evaluate the effect of RA on WEC formation and crack morphology. The outcomes can be derived based on the findings of the present study are as follows:

- Low carbon potential carburizing and high-temperature tempering resulted in the decrease in surface hardness for low RA samples.
- Varying the RA level caused drastic differences in the morphology of the WECs which developed within the samples.
- Samples with higher levels of RA contained far more branching crack networks, and the WEA adjacent to the crack networks was less defined. This shows positive impact of RA on WEC formation.

This study confirms that subsurface crack-initiated spalling can occur originally due to WEC formation and eventually can lead to catastrophic premature component failure. The study contributes significantly to the existing literature about

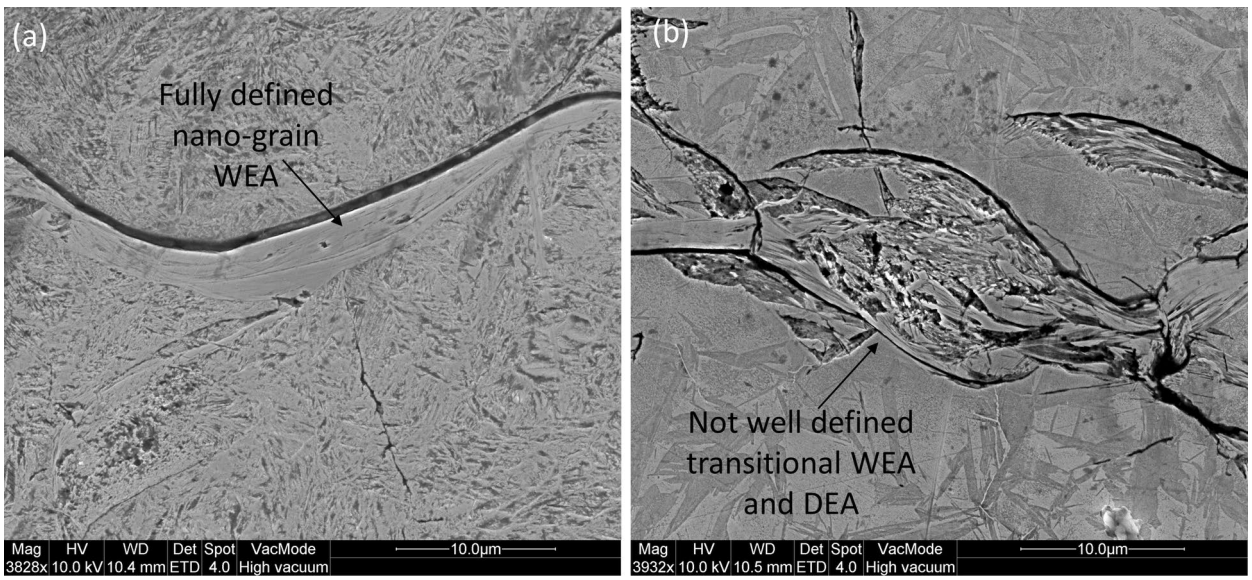

Fig. 9 Two SEM images showing the differences in the appearance of the WEA within the low RA samples (**a**) and the high RA samples (**b**)

the role of RA on WEC behavior under boundary lubrication which is mainly observed in wind turbine but can also be noted in agricultural machineries as well as earth moving equipments.

Acknowledgements The authors would like to thank Dr. Maria De La Cinta Lorenzo Martin for her assistance with electron microscopy and Dr. Oyelayo Ajayi for his helpful discussion on metallurgy. Present study is a part of Project funded by John Deere Product Engineering Center in Waterloo, Iowa and Iowa State University. This work was also supported by the US Department of Energy Office of Energy Efficiency and Renewable Energy, Wind Energy Technology Office under Contract No. DE-AC02-06CH11357. The authors are grateful to DOE Project Managers Mr. Michael Derby and Mr. Brad Ring for their support and encouragement. Use of the Center for Nanoscale Materials an Office of Science User Facility was supported by the US Department of Energy Office of Science, Office of Basic Energy Sciences under Contract No. DE-AC02-06CH11357.

References

1. Kotzalas, M.N., Doll, G.L.: Tribological advancements for reliable wind turbine performance. Philos. Trans. **368**(1929), 4829–4850 (2010)
2. Musial, W., Butterfield, S., McNiff, B.: Improving wind turbine gearbox reliability. In: European Wind Energy Conference, 2007, Milan Italy, pp. 7–10
3. Greco, A., et al.: Material wear and fatigue in wind turbine systems. Wear **302**(1–2), 1583–1591 (2013)
4. Singh, H., et al.: Investigation of microstructural alterations in low- and high-speed intermediate-stage wind turbine gearbox bearings. Tribol. Lett. **65**(3), 81 (2017)
5. Kang, J.H., et al.: Solute redistribution in the nanocrystalline structure formed in bearing steels. Scr. Mater. **69**(8), 630–633 (2013)
6. Smelova, V., et al.: Electron microscopy investigations of microstructural alterations due to classical Rolling Contact Fatigue (RCF) in martensitic AISI 52100 bearing steel. Int. J. Fatigue **98**, 142–154 (2017)
7. Smelova, V., et al.: Microstructural changes in White Etching Cracks (WECs) and their relationship with those in Dark Etching Region (DER) and White Etching Bands (WEBs) due to Rolling Contact Fatigue (RCF). Int. J. Fatigue **100**, 148–158 (2017)
8. Su, Y.-S., et al., Review of the damage mechanism in wind turbine gearbox bearings under rolling contact fatigue. Front. Mech. Eng. (2017). https://doi.org/10.1007/s11465-018-0474-1
9. Su, Y.S., et al.: Deformation-induced amorphization and austenitization in white etching area of a martensite bearing steel under rolling contact fatigue. Int. J. Fatigue **105**, 160–168 (2017)
10. Gould, B., Greco, A.: The influence of sliding and contact severity on the generation of white etching cracks. Tribol. Lett. **60**(2), 29 (2015)
11. Grabulov, A., Petrov, R., Zandbergen, H.W.: EBSD investigation of the crack initiation and TEM/FIB analyses of the microstructural changes around the cracks formed under Rolling Contact Fatigue (RCF). Int. J. Fatigue **32**(3), 576–583 (2010)
12. Grabulov, A., Ziese, U., Zandbergen, H.W.: TEM/SEM investigation of microstructural changes within the white etching area under rolling contact fatigue and 3-D crack reconstruction by focused ion beam. Scr. Mater. **57**(7), 635–638 (2007)
13. Martin, J.A., Borgese, S.F., Ad, E.: Microstructural alterations of rolling—bearing steel undergoing cyclic stressing. J. Basic Eng. **88**(3), 555 (1966)
14. Obrien, J.L., King, A.H.: Electron microscopy of stress-induced structural alterations near inclusions in bearing steels. J. Basic Eng. **88**(3), 568 (1966)
15. Lund, T.B., Beswick, J., Dean, S.W.: Sub-surface initiated rolling contact fatigue—influence of non-metallic inclusions. J. ASTM Int. **7**(5), 102559 (2010)
16. Scott, D., Loy, B., Mills, G.H.: Paper 10: metallurgical aspects of rolling contact fatigue. In: Proceedings of the Institution of Mechanical Engineers, pp. 94–103. SAGE Journals (1966)
17. Stadler, K., Lai, J., Vegter, R., A review: the dilemma with premature white etching crack (WEC) bearing failures. In: Bearing Steel Technologies: Advances in Steel Technologies for Rolling Bearings, vol. 10, pp. 487–508. ASTM International, West Conshohocken (2015)
18. Evans, M.H.: An updated review: white etching cracks (WECs) and axial cracks in wind turbine gearbox bearings. Mater. Sci. Technol. **32**(11), 1133–1169 (2016)
19. Luyckx, J.: Hammering wear impact fatigue hypothesis WEC/irWEA failure mode on roller bearings. In: NREL Wind Tribology Seminar (2011)
20. Hyde, S.: White etch areas: metallurgical characterization and atomistic modeling (2014)
21. Solano-Alvarez, W., Bhadeshia, H.K.D.H.: White-etching matter in bearing steel. Part II: distinguishing cause and effect in bearing steel failure. Metall. Mater. Trans. A **45a**(11), 4916–4931 (2014)
22. Bhadeshia, H.K.D.H.: Steels for bearings. Prog. Mater. Sci. **57**(2), 268–435 (2012)
23. Evans, M.H., et al.: Serial sectioning investigation of butterfly and white etching crack (WEC) formation in wind turbine gearbox bearings. Wear **302**(1–2), 1573–1582 (2013)
24. Bruce, T., et al.: Characterisation of white etching crack damage in wind turbine gearbox bearings. Wear **338**, 164–177 (2015)
25. Gould, B., Greco, A.: Investigating the process of white etching crack initiation in bearing steel. Tribol. Lett. **62**(2), 26 (2016)
26. Errichello, R., et al.: Wind Turbine Tribology Seminar: A Recap (2011)
27. Gegner, J.: Tribological Aspects of Rolling Bearing Failures. INTECH Open Access Publisher, London (2011)
28. Loos, J., Bergmann, I., Goss, M.: Influence of currents from electrostatic charges on WEC formation in rolling bearings. Tribol. Trans. **59**(5), 865–875 (2016)
29. Gould, B.J., Burris, D.L.: Effects of wind shear on wind turbine rotor loads and planetary bearing reliability. Wind Energy **19**, 1011–1021 (2015)
30. Garabedian, N., et al.: The cause of premature wind turbine bearing failures: overloading or underloading? Tribol. Trans. **61**(5), 850–860 (2018)
31. Kang, Y.S., Evans, R.D., Doll, G.L.: Roller-raceway slip simulations of wind turbine gearbox bearings using dynamic bearing model. In: Proceedings of the STLE/ASME International Joint Tribology Conference, 2010, pp. 407–409 (2011)
32. Holweger, W.: Progresses in Solving White Etching Crack Phenomena. NREL: Gearbox Reliability Collaborative, Golden (2014)
33. Strandell, I., Fajers, C., Lund, T.: Corrosion—one root cause for premature failures. In: 37th Leeds–Lyon Symposium on Tribology (2010)
34. Iso, K., Yokouchi, A., Takemura, H.: Research Work for Clarifying the Mechanism of White Structure Flaking and Extending the Life of Bearings. SAE Technical Paper, 2005(SP-1967), pp. 39–48
35. Vegter, R.H., Slycke, J.T.: The role of hydrogen on rolling contact fatigue response of rolling element bearings. J. ASTM Int. **7**(2), 1–12 (2010)
36. Uyama, H., et al.: The effects of hydrogen on microstructural change and surface originated flaking in rolling contact fatigue. Tribol. Online **6**, 123–132 (2011)

37. Hiraoka, K., et al.: Generation process observation of microstructural change in rolling contact fatigue by hydrogen-charged specimens. J. Jpn. Soc. Tribol. **52**(12), 888–895 (2007)
38. Kino, N., Otani, K.: The influence of hydrogen on rolling contact fatigue life and its improvement. JSAE Rev. **24**(3), 289–294 (2003)
39. Tamada, K., Tanaka, H.: Occurrence of brittle flaking on bearings used for automotive electrical instruments and auxiliary devices. Wear **199**(2), 245–252 (1996)
40. Ciruna, J.A., Szieleit, H.J.: The effect of hydrogen on the rolling contact fatigue life of AISI 52100 and 440C steel balls. Wear **24**, 107–118 (1973)
41. Grunberg, L.: The formation of hydrogen peroxide on fresh metal surfaces. Proc. Phys. Soc. Lond. B **66**(399), 153–161 (1953)
42. Imran, T., Jacobson, B., Shariff, A.: Quantifying diffused hydrogen in AISI-52100 bearing steel and in silver steel under tribomechanical action: pure rotating bending, sliding–rotating bending, rolling–rotating bending and uni-axial tensile loading. Wear **261**(1), 86–95 (2006)
43. Ray, D., et al.: Hydrogen embrittlement of a stainless ball-bearing steel. Wear **65**(1), 103–111 (1980)
44. Matsubara, Y., Hamada, H.: A novel method to evaluate the influence of hydrogen on fatigue properties of high strength steels. J. ASTM Int. **3**, 1–14 (2006)
45. Lu, H., et al.: Hydrogen-enhanced dislocation emission, motion and nucleation of hydrogen-induced cracking for steel. Sci. China E **40**(5), 530–538 (1997)
46. Fujita, S., et al.: Effect of hydrogen on Mode II fatigue crack behavior of tempered bearing steel and microstructural changes. Int. J. Fatigue **32**(6), 943–951 (2010)
47. Evans, M.H., et al.: Effect of hydrogen on butterfly and white etching crack (WEC) formation under rolling contact fatigue (RCF). Wear **306**(1–2), 226–241 (2013)
48. Ruellan, A., et al.: Understanding white etching cracks in rolling element bearings: the effect of hydrogen charging on the formation mechanisms. Proc. Inst. Mech. Eng. J **228**, 1252–1265 (2014)
49. Evans, M.H., et al.: White etching crack (WEC) investigation by serial sectioning, focused ion beam and 3-D crack modelling. Tribol. Int. **65**, 146–160 (2013)
50. Guzman, F.G., et al.: Reproduction of white etching cracks under rolling contact loading on thrust bearing and two-disc test rigs. Wear **390–391**, 23–32 (2017)
51. Danielsen, H.K., et al.: Multiscale characterization of White Etching Cracks (WEC) in a 100Cr6 bearing from a thrust bearing test rig. Wear **370**, 73–82 (2017)
52. Richardson, A.D., et al.: The evolution of white etching cracks (WECs) in rolling contact fatigue-tested 100Cr6 steel. Tribol. Lett. **66**(1), 6 (2018)
53. Richardson, A.D., et al.: Thermal desorption analysis of hydrogen in non-hydrogen-charged rolling contact fatigue-tested 100Cr6 steel. Tribol. Lett. **66**(1), 4 (2018)
54. Scepanskis, M., Gould, B., Greco, A.: Empirical investigation of electricity self-generation in a lubricated sliding–rolling contact. Tribol. Lett. **65**, 109–119 (2017)
55. Evans, M.H., et al.: Confirming subsurface initiation at non-metallic inclusions as one mechanism for white etching crack (WEC) formation. Tribol. Int. **75**, 87–97 (2014)
56. Franke, J., et al.: White etching cracking—simulation in bearing rig and bench tests. Tribol. Trans. **61**(3), 403–413 (2018)
57. Gould, B., et al.: The effect of lubricant composition on white etching crack failures. Tribol. Lett. 67(7), 7 (2019)
58. Paladugu, M., Hyde, R.S.: White etching matter promoted by intergranular embrittlement. Scr. Mater. **130**, 219–222 (2017)
59. Paladugu, M., Hyde, R.S.: Microstructure deformation and white etching matter formation along cracks. Wear **390–391**, 367–375 (2017)
60. Li, S.X., et al.: Microstructural evolution in bearing steel under rolling contact fatigue. Wear **380–381**, 146–153 (2017)
61. Bruce, T., et al.: Formation of white etching cracks at manganese sulfide (MnS) inclusions in bearing steel due to hammering impact loading. Wind Energy **19**(10), 1903–1915 (2016)
62. Gould, B., et al.: An analysis of premature cracking associated with microstructural alterations in an AISI 52100 failed wind turbine bearing using X-ray tomography. Mater. Des. **117**, 417–429 (2017)
63. Gould, B., et al.: Using advanced tomography techniques to investigate the development of White Etching Cracks in a prematurely failed field bearing. Tribol. Int. **116**, 362–370 (2017)
64. Errichello, R., Budny, R., Eckert, R.: Investigations of bearing failures associated with white etching areas (WEAs) in wind turbine gearboxes. Tribol. Trans. **56**(6), 1069–1076 (2013)
65. Paladugu, M., Hyde, R.S.: Influence of microstructure on retained austenite and residual stress changes under rolling contact fatigue in mixed lubrication conditions. Wear **406–407**, 84–91 (2018)
66. Ooi, G.T.C., Roy, S., Sundararajan, S.: Investigating the effect of retained austenite and residual stress on rolling contact fatigue of carburized steel with XFEM and experimental approaches. Mater. Sci. Eng. A **732**, 311–319 (2018)
67. Roy, S., Ooi, G.T.C., Sundararajan, S.: Effect of retained austenite on micropitting behavior of carburized AISI 8620 steel under boundary lubrication. Materialia **3**, 192–201 (2018)
68. Roy, S., Sundararajan, S.: Effect of retained austenite on spalling behavior of carburized AISI 8620 steel under boundary lubrication. Int. J. Fatigue **119**, 238–246 (2019)
69. Roy, S., Sundararajan, S.: The effect of heat treatment routes on the retained austenite and tribomechanical properties of carburized AISI 8620 steel. Surf. Coat. Technol. **308**, 236–243 (2016)
70. Roy, S., White, D., Sundararajan, S.: Correlation between evolution of surface roughness parameters and micropitting of carburized steel under boundary lubrication condition. Surf. Coat. Technol. **350**, 445–452 (2018)
71. Singh, H., et al.: Fatigue resistant carbon coatings for rolling/sliding contacts. Tribol. Int. **98**, 172–178 (2016)
72. Chung, Y.-W.: Introduction to Materials Science and Engineering. CRC Press, Boca Raton (2006)
73. Zeng, D., et al.: Influence of laser dispersed treatment on rolling contact wear and fatigue behavior of railway wheel steel. Mater. Des. **54**, 137–143 (2014)
74. Dommarco, R.C., et al.: Residual stresses and retained austenite evolution in SAE 52100 steel under non-ideal rolling contact loading. Wear **257**(11), 1081–1088 (2004)
75. Evans, M.H.: White structure flaking (WSF) in wind turbine gearbox bearings: effects of 'butterflies' and white etching cracks (WECs). Mater. Sci. Technol. **28**(1), 3–22 (2012)
76. Osterlund, R., et al.: Butterflies in fatigued all bearings—formation mechanism and structure. Scand. J. Metall. **11**, 23–32 (1982)